Application of Mie Light Scattering to the Morphological Development of Polypropylene/Polystyrene Blends. I. Method for the Determination of Mie Scattering

Yun Yan Li, Da Yan, Gui Qiu Ma, Xu Bo Yuan, Jing Sheng

Tianjin Key Laboratory of Composite and Functional Materials, School of Material Science and Engineering, Tianjin University, Tianjin, 300072, China

Received 22 February 2009; accepted 4 July 2009
DOI 10.1002/app.31074
Published online 7 January 2010 in Wiley InterScience (www.interscience.wiley.com).

ABSTRACT: In this article, we introduce a new method, Mie scattering, for investigating the dependence of the morphology of polypropylene (PP)/polystyrene (PS) blends on the composition and mixing time. The size and corresponding distribution of the particles were also deduced on the basis of the Mie scattering theory. To confirm the effectiveness of this new method for morphology studies, scanning electron microscopy (SEM) was employed to study the morphology development as a function of the blend composition and mixing time; furthermore, the results by Mie scattering were compared with those by SEM analysis. The results by Mie scattering were similar to those by SEM, and this indicated that Mie scattering is an effective method for describing the morphology development of polymer blends. The main purpose of this article is simply to report this new method; in another article of this series, the application of this method in investigations of the compatibilization of PP/PS blends will be reported. © 2010 Wiley Periodicals, Inc. J Appl Polym Sci 116: 1933–1939, 2010

Key words: microstructure; particle size distribution; poly(propylene) (PP); polystyrene

INTRODUCTION

Because the morphology development of polymer blends has a significant influence on their mechanical properties, the mechanism of morphology development has attracted much interest from both academic and commercial institutions. During the past few decades, many research groups have carried out corresponding studies to gain a better understanding of morphology development, and good results have been found.[1–18] Favis[11] studied the mixing process using an intermittent mixer and found that the change in the phase morphology occurred mainly within the first 2 min. Scott and Macosko[9] investigated the phase transformation in the initial stage of the blending process using an intermittent mixer, a single-screw extruder, and a twin-screw extruder and obtained similar results. To observe the phase formation and evolution with time, Shih[19] opened a window on the mixer and observed the macroscopic structural changes with a video, which cannot be used to study the microscopic structure of the phase morphology. Zou et al.[20] examined the phase evolution of polystyrene (PS)/poly(*cis*-butadiene) rubber by sampling during melting and mixing and determined the changing regulations of the dispersed phase.

It is well known that when two immiscible/incompatible polymers are blended, one phase will mechanically disperse into the other and form the dispersed phase, whereas the other will become the continuous phase. In general, the domain size of the minor phase depends greatly on the composition, the viscoelasticity of the constituent components, the shear stress/rate, and the interfacial tension between phases. Therefore, the phase morphology can be controlled by the adjustments of processing conditions (e.g., the mixing temperature and the rotor speed) and the miscibility between phases by the introduction of a suitably chosen copolymer.

In most past studies, scanning electron microscopy (SEM) and related image analysis technology have been widely employed for the following reasons. For a multiphase polymer, the microimage of the phase morphology represents the spatial distribution and temporal evolution of parameters such as the concentration and tropism; furthermore, the formation and selection of the pattern correspond to the phase formation and evolution of polymer blends, respectively. Therefore, the analysis of SEM images is an effective way to study the phase formation and

Correspondence to: J. Sheng (shengjing@tju.edu.cn).
Contract grant sponsor: National Natural Science Foundation of China; contract grant number: 50390090.
Contract grant sponsor: Scientific and Technological Committee of Tianjin City, China; contract grant number: 05YFJMJC09100.

evolution during the mixing process. Unfortunately, SEM is not a very convenient way because one must spend much time processing the SEM images, extracting effective information from the images, and calculating the structural parameters. In this case, many other technologies, such as small-angle light scattering, have been developed and applied with or without the combination of SEM. Because very systematic and precise light-scattering theories have been developed, it is effective to study blend structures by means of small-angle light scattering. In past studies, Rayleigh light scattering has been used to investigate the morphology development of various polymer blends, and better results have been obtained. In comparison with the Rayleigh theory, Mie scattering, which can also be used to describe blend structures, has been rarely used. Therefore, in this article, a new method, that is, Mie scattering, is introduced and applied to the study of the composition/mixing time dependence of the phase morphology of polypropylene (PP)/PS blends during mixing; we are aiming to provide a new method for studying the morphology of polymer blends.

EXPERIMENTAL

Materials

The basic materials used in this study were commercial-grade PP (1300) with a density of 0.91 g/cm^3, a weight-average molecular weight of 5.0×10^5 g/mol, and a melting temperature of 178°C and a commercial-grade PS (666D) with a density of 1.05 g/cm^3, a weight-average molecular weight of 5.8×10^5 g/mol, and a glass-transition temperature of 111°C. All these materials were supplied by Beijing Yanshan Petrochemical (Beijing, China).

Blend preparation

PP and PS were blended in a batch internal mixer with a rotor diameter of 35 mm (XXS-300 torque rheometer, KeChuang Machinery, Shanghai, China). Before processing, all materials were dried for 8–10 h *in vacuo* at 70°C. To investigate the composition dependence of the domain size of the dispersed phase, PP and PS were blended in different weight ratios at 190°C and at a rotor speed of 32 rpm. The compositions of the PP/PS blends used in this study ranged from 10/90 to 90/10. Furthermore, the effect of the mixing time on the morphology was also studied, and for this purpose, samples were taken out of the mixer at different mixing times and were immediately quenched in liquid nitrogen to freeze the original structure for observation in a scanning electron microscope.

Morphological characterization

A scanning electron microscope (XL30, Philips, Amsterdam, Netherland) operated at an accelerating voltage of 20 kV was used to examine the fracture surface morphology of the blends. The preblended samples were broken in liquid nitrogen, and the fracture surface was covered with gold for observation in the microscope. To make sure that the original structure of the blends was intact, the surface was not etched.

The morphology was quantified with special software. On each SEM image, the contour and mass center of each domain were detected; each domain was scanned by straight lines going through the mass center from different directions; and the span from one side of a domain to the other, which is defined as diameter d_g in this article, was noted by a computer. Consequently, the average size of the domains could be calculated by the averaging of these d_g values with eq. (1):

$$(d_g)_m = \frac{\sum_i^\infty n_i (d_g)_i}{\sum_i^\infty n_i} \quad (1)$$

where $(d_g)_m$ is the average diameter, with m being "mean", and n_i is the number of particles with diameter $(d_g)_i$).

To obtain more reliable data, about 500 domains were considered to calculate these structural parameters for each sample. Because the quality and resolution of SEM images are strongly affected by the thickness of the plated gold, the sputter time was strictly controlled to be the same for each sample.

Small angle light back scattering (SALBS) analysis

The whole mixing process was also investigated with a backscattering apparatus constructed at Tianjin University (Tianjin, China). Figure 1 presents a schematic representation of the apparatus. The SALBS apparatus consisted of eight parts. A He–Ne laser was used as an incident light source [wave length (A_0) = 6328 A]. The parallel beam was filtered by a filter to change the intensity of the incident light. The polarization direction of the laser beam could be varied by the rotation of a polarizer. The incident beam was reflected by a half-reflecting and half-transmitting mirror and irradiated the sample. The backscattered light from the sample was passed through the mirror, optical system, and

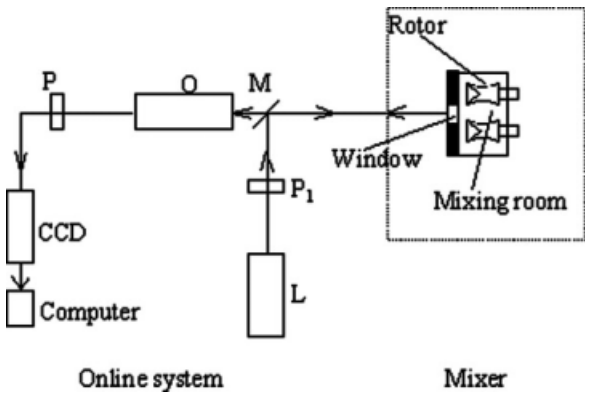

Figure 1 Schematic representation of the light-scattering system (L = He–Ne laser; P_1 = polarizer; M = half-reflecting and half-transmitting mirror; O = optical system; CCD = charged coupling device).

polarization analyzer and was detected by a charged coupling device connected to a computer. The optical system was specially designed not to broaden the laser beam. Thus, the reflected element depended only on the diameter of the laser beam, which covered a small angle (<0.5°).

Mie scattering theory

According to the Mie scattering theory,[21] when an incident beam of wavelength λ reaches a spherical domain with diameter D, the scattering of radiation by the spherical domain is related to the incident beam as follows:

$$I = \frac{\lambda^2}{8\pi^2 r^2} I_0(i_1 + i_2) = \left(\frac{\lambda}{2\pi r}\right)^2 I_0 \frac{i_1 + i_2}{2} = \frac{i_1 + i_2}{2k^2 r^2} I_0 \quad (2)$$

where I is the intensity of the scattering beam and k is the wave number ($k = 2\pi/\lambda$), I_0 is the intensity of the incident beam, and r is the scattering distance between the domain and a receiver on which the scattering image is displayed. i_1 and i_2 are the intensities of the beams that vibrate perpendicularly and parallel to the plane determined by the scattering and incident beams, respectively:

$$i_1 = |S_1(\theta)|^2, i_2 = |S_2(\theta)|^2 \quad (3)$$

$$S_1(\theta) = \sum_{n=1}^{\infty} \frac{2n+1}{n(n+1)} [a_n \pi_n(\cos\theta) + b_n \tau_n(\cos\theta)] \quad (4a)$$

$$S_2(\theta) = \sum_{n=1}^{\infty} \frac{2n+1}{n(n+1)} [b_n \pi_n(\cos\theta) + a_n \tau_n(\cos\theta)] \quad (4b)$$

where S_1, S_2 are the scattering vectors which are perpendicular and parallel to the plane determined by the scattering and incident beams, respectively; θ is the angle between the direction of the incident and scattered radiation (scattering angle). Coefficients a_n, b_n, π_n, and τ_n can be theoretically obtained as follows:

$$a_n = \frac{\psi'_n(y)\psi_n(x) - m\psi_n(y)\psi'_n(x)}{\psi'_n(y)\zeta_n(x) - m\psi_n(y)\zeta'_n(x)} \quad (5a)$$

$$b_n = \frac{m\psi'_n(y)\psi_n(x) - \psi_n(y)\psi'_n(x)}{m\psi'_n(y)\zeta_n(x) - \psi_n(y)\zeta'_n(x)} \quad (5b)$$

where

$$\psi_n(z) = \left(\frac{z\pi}{2}\right)^{\frac{1}{2}} J_{n+\frac{1}{2}}(z) \quad (6a)$$

$$\zeta_n(z) = \left(\frac{z\pi}{2}\right)^{\frac{1}{2}} H^{(2)}_{n+\frac{1}{2}}(z) \quad (6b)$$

$J_{n+1/2}(z)$ and $H^{(2)}_{n+1/2}(z)$ are the first Bessel function and second Hanker function, respectively, and $\psi'_n(z)$ and $\zeta'_n(z)$ are the first derivatives of $\psi_n(z)$ and $\zeta_n(z)$, respectively. In eq. (4), π_n and τ_n are determined only by the scattering angle as follows:

$$\pi_n(\cos\theta) = \frac{1}{\sin\theta} P'_n(\cos\theta) = \frac{dP_n(\cos\theta)}{d(\cos\theta)} \quad (7a)$$

$$\tau_n(\cos\theta) = \frac{d}{d\theta} P'_n(\cos\theta) \quad (7b)$$

where π_n and τ_n are the Riccati and Bessel functions, respectively; P'_n is the first derivative of the Legendre function P'_n; and $x = ka$ and $y = mka$ (m is the refraction index, and a is the radius of the scattering domains).

If we define ξ as cos θ, eq. (7) can be transformed into the following:

$$\pi_n = \frac{dP_n(\xi)}{d\xi} = P'_n(\xi) \quad (8)$$

$$\tau_n = \frac{d}{d\theta} P'_n(\xi) \quad (9)$$

Because

$$P'_n(\xi) = (1-\xi^2)^{\frac{1}{2}} \frac{d}{d\xi} P_n(\xi) = (1-\xi^2)^{\frac{1}{2}} \pi_n \quad (10)$$

$$d\theta = \frac{1}{\sin\theta} d\xi = -(1-\xi^2)^{\frac{-1}{2}} d\xi$$

we can obtain

$$\tau_n = \xi\pi_n - (1-\xi^2)\pi_n \quad (11)$$

The recurrence relationship of the Legendre function is[22]

$$P_{n+1}(\xi) = \frac{2n+1}{n+1}\xi P_n(\xi) - \frac{n}{n+1}P_{n-1}(\xi) \quad (12a)$$

$$P'_{n+1}(\xi) - P'_{n-1}(\xi) = (2n+1)P_n(\xi) \quad (12b)$$

$$(\xi^2 - 1)P'_n(\xi) = n\xi P_n(\xi) - nP_{n-1}(\xi) \quad (12c)$$

$$nP_n(\xi) = \xi P'_n(\xi) - P'_{n-1}(\xi) \quad (12d)$$

Combining eqs. (8) and (9) and eq. (12), we can obtain

$$\pi_n = \frac{2n-1}{n-1}\xi\pi_{n-1} - \frac{n}{n-1}\pi_{(n-2)} \left| \begin{matrix} \pi_0 = 0 \\ \pi_1 = 1 \end{matrix} \right. \quad (13a)$$

$$\tau_n = n\xi\pi_n - (n+1)\pi_{(n-1)} \quad (13b)$$

From eq. (5), as long as the recurrence functions of $\psi_n(z)$ and $\zeta_n(z)$ are obtained, a_n and b_n can be easily obtained. Generally, both the Bessel and Hanker functions comply with the following recurrence relationship:[22]

$$Y_{n+1}(z) = \frac{2n}{z}Y_n(z) - Y_{n-1}(z) \quad (14a)$$

$$Y'_n(z) = \frac{1}{2}[Y_{n-1}(z) - Y_{n+1}(z)] \quad (14b)$$

Substituting eq. (14) into eq. (6), we can obtain the following group of functions:

$$\left\{ \begin{array}{l} \psi_n(z) = \frac{2n-1}{z}\psi_{n-1}(z) - \psi_{n-2}(z) \\ \zeta_n(z) = \frac{2n-1}{z}\zeta_{n-1}(z) - \zeta_{n-2}(z) \\ \psi'_n(z) = \psi_{n-1}(z) - \frac{n}{z}\psi_n(z) \\ \zeta'_n(z) = \zeta_{n-1}(z) - \frac{n}{z}\zeta_n(z) \end{array} \right\} \quad \text{and}$$

$$\left\{ \begin{array}{l} \psi_0(z) = \sin z \\ \psi_1(z) = \frac{1}{z}\sin z - \cos z \\ \zeta_0(z) = \sin z + i\cos z \\ \zeta_1(z) = \frac{1}{z}(\sin z + i\cos z) - (\cos z - i\sin z) \\ = \psi_1(z) + i(\frac{\cos z}{z} + \sin z) \end{array} \right\} \quad (15)$$

With the aforementioned function group, $\psi_n(a)$, $\psi'_n(a)$, $\psi_n(ma)$, $\zeta_n(a)$, and $\zeta'_n(a)$ can be calculated, and a_n and b_n can be further obtained.

Determination of the domain size and distribution

For scattering units with a periodic structure, spinodal rings always can be observed on the scattering image, and the relationship between the periodic structure and the scattering vector always complies with the following:

$$\Lambda_m(t) = 2\pi h_{sm}(t) \quad (16)$$

where $\Lambda_m(t)$ is the periodic dimension and $h_{sm}(t)$ is the scattering vector at which the peak of the scattering intensity (the spinodal ring) appears. If there are several periodic structures, the same number of spinodal rings appears on the scattering image; that is, the spinodal ring has a one-by-one relationship with the periodic structure. From the scattering image, $h_{sm}(t)$ can be easily obtained, and then $\Lambda_m(t)$ or domain diameter d_i can be calculated with eqs. (17) and (18), in which ϕ_{di} is the domain number with diameter d_i:

$$\Lambda_m(t) = 2\pi h_{sm}^{-1}(t) \quad (17)$$

$$d_i(t) = \frac{3\Lambda_m(t)}{2(1 - \phi_{d_i})} \quad (18)$$

For a system in which the minor phase is dispersed in the form of domains of different sizes, the Mie scattering theory can be applied to determine the polydispersity of the phase dimension. If we take into account that the scattering intensities by different domains are not correlated, the total scattering intensity at scattering angle θ_k is

$$I(\theta_k) = \sum_i N_i I(d_i, \theta_k) \quad (19)$$

where $I(d_i,\theta_k)$ is the scattering intensity by a single domain of d_i and N_i is the corresponding number of domain i. Similarly, the relative domain number with specific size d_i can be calculated by the resolution of a linear function group as long as the domain size and scattering intensity at θ_k are determined.

RESULTS AND DISCUSSION

SEM images of PP/PS with different compositions at 10 min are shown in Figure 2. Because of the poor cohesion between PP and PS, domains of the dispersed phase were completely pooled out, leaving cavities or balloons dispersed in the matrix when broken. For a lower concentration of the dispersed phase, the typical domain dispersion morphology could be observed; that is, PP or PS was distributed in the matrix in the form of spherical domains, one forming the dispersed phase and the other forming the continuous phase. Qualitatively, the phase dimension became large with the concentration of the dispersed phase and formed a special cocontinuous structure, which is described in detail by digital image analysis (DIA) and Mie scattering theory later.

Furthermore, we can observe that, when PP was the dispersed phase, a cocontinuous structure appeared early even in blends in which the concentration of PP was only 30 wt %. However, the occurrence of a cocontinuous structure was prolonged

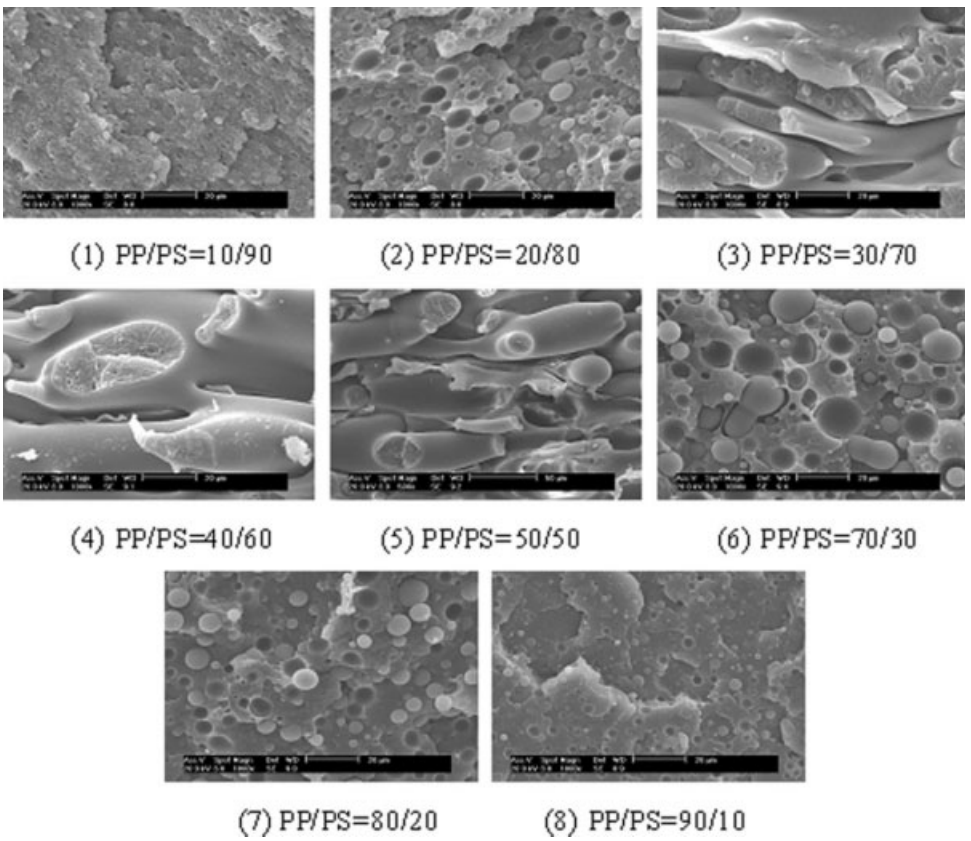

Figure 2 SEM images of PP/PS with different compositions at 10 min.

until the concentration of the dispersed phase was 50% when PS acted as the dispersed phase. This interesting result might have resulted from the differences in the physical properties of PP and PS, especially the melt viscosity.

To study the relationship between the blend composition and the corresponding morphology quantitatively, DIA and Mie scattering were used in this study. In Figure 3, the domain diameters for different compositions are shown. The domain size of the dispersed phase increased with the concentration of the dispersed phase, and furthermore, more attention should be paid to the fact that the increase in the domain size was not very apparent when the volume fraction of PS was lower than 20%; only when the fraction of PS was higher than 20% did the domain size increase rapidly because of the dynamic coalescence between different domains. In this study, similar results were obtained for different blends, and these results could be ascribed to the adequate space that could be used to accommodate new domains resulting from the addition of a concentration of the dispersed phase. However, the further addition of the dispersed phase fully took up all the space and led to coalescence between domains, leading to a rapid increase in the domain size.

As mentioned previously, between 30% and 50% PP, the PP/PS blends showed a continuous structure, and this can also be supported by the results from DIA. Unfortunately, the results of Mie scattering tell us that the PP/PS blends still had a domain-dispersion morphology and corresponding structural parameter; for example, the domain diameter could be easily obtained, and this is not the truth. Therefore, it is not appropriate to apply the Mie scattering theory to determine the cocontinuous region. Furthermore, as we can observe, there is much difference between the results from SEM digital

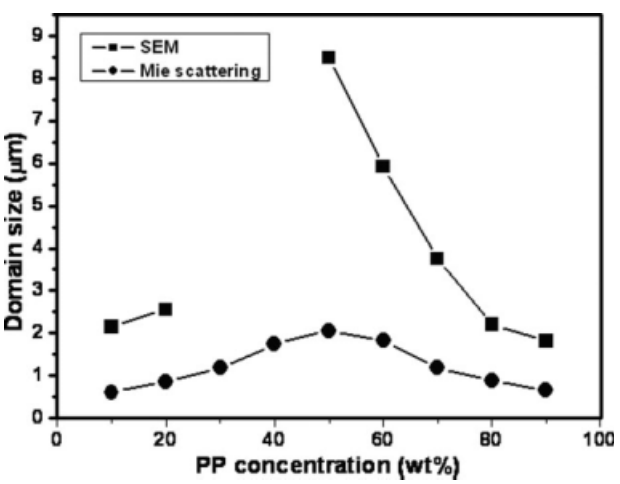

Figure 3 Domain diameters for different compositions.

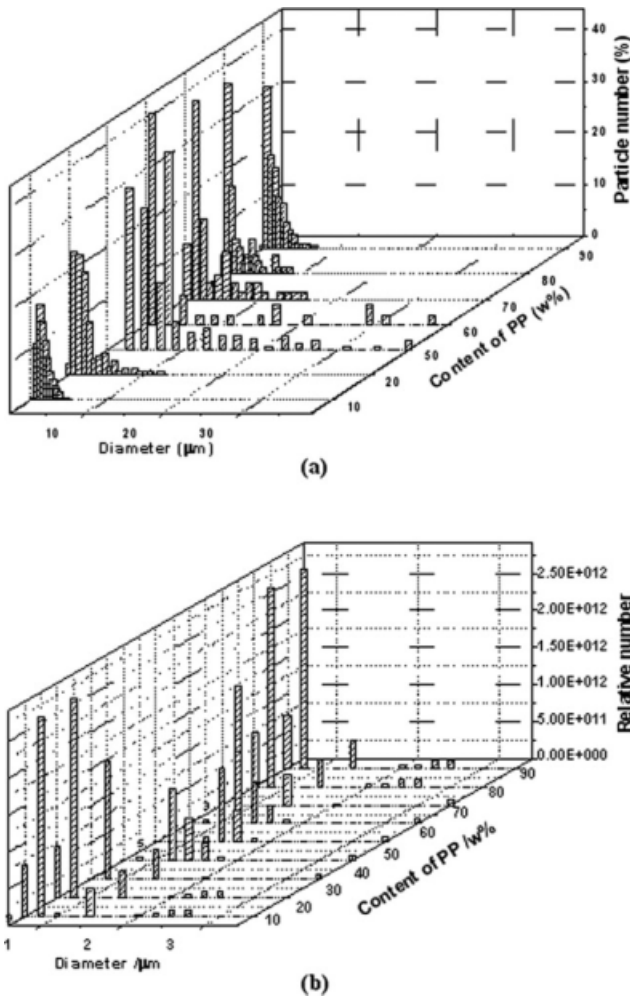

Figure 4 Bar diagrams of the size distributions for different blend compositions by (a) SEM and (b) Mie scattering.

analysis and Mie scattering: the values by SEM were larger than those by Mie scattering. We believe that this difference mainly resulted from unavoidable coalescence when the mixer window was opened after the machine was stopped; that is, there was a longer time between the stopping of the machine and the quench hardening of the samples in liquid nitrogen, during which the dispersed domain had a higher coalescence efficiency resulting from the smaller domain size and higher interfacial tension. Consequently, adjacent smaller domains coalesced with one another to form larger ones. For this reason, the domain size from SEM was larger than that from Mie scattering. Furthermore, there might be other reasons for this difference, such as the limitations of the Mie theory and calculation variations. Detailed research has recently been carried out by our group to provide a better explanation, but unfortunately, no further information has been obtained yet.

In Figure 4, bar diagrams of the size distributions for different blend compositions are shown. As the concentration of the dispersed phase increased, the domain size distribution became poor, and this was accompanied by an increase in the domain size, which agreed with the SEM images. Actually, with an increase in the concentration of the minor phase, the number of smaller domains and the collision probability increased, and this led to coalescence between smaller domains. According to the dynamic equilibrium between breaking and coalescence, the domains should have had a regular spherical shape even when the concentration of the dispersed phase was higher; however, an apparent percolation structure appeared for 30% PP (see Fig. 2). This might be due to the extra domain number. If we suppose that under dynamic equilibrium most domains have a regular shape, a temporary percolation structure will form when two domains collide with each other; unfortunately, this percolation will be quickly broken by the strong shear stress into two smaller domains, and so these two new domains will collide again with others because of the extra domain number and the consequently high collision probability. This interesting circulation will be continuous throughout the whole mixing process, and consequently, the percolation structure will exist all the time. Furthermore, the size distribution by Mie scattering was similar to that by SEM, and this indicates that Mie scattering is effective for describing the size and distribution of polymer bends; for this reason, we studied the relationship between the mixing time and blend structure to confirm the validity of Mie scattering in studies related to polymer structure.

Variations of the domain size as a function of the mixing time are shown in Figure 5. As expected, the domain size decreased in the initial stage. This indicates that the breakup of the dispersed domains was predominant initially. In the late stage, with an increase in coalescence arising from forced collisions

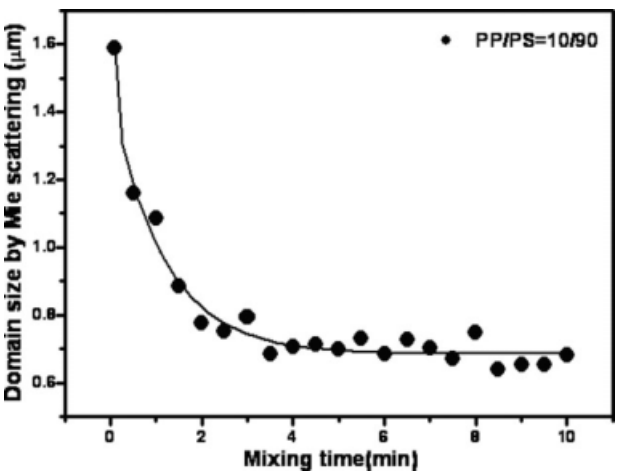

Figure 5 Variation of the domain size by the Mie theory as a function of the mixing time.

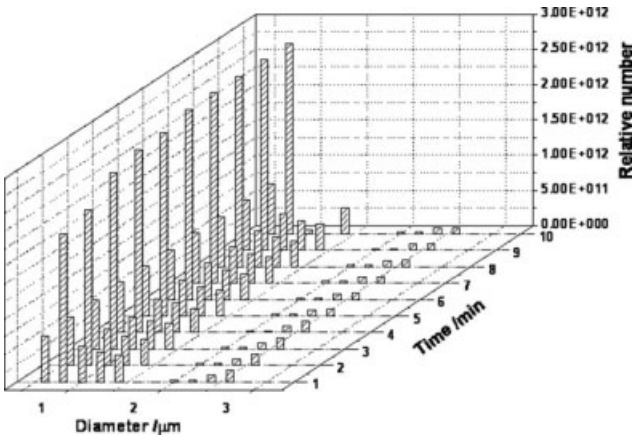

Figure 6 Bar diagram of the diameter distribution at different mixing times by Mie scattering.

of the dispersed domains during mixing, the domain size leveled off, and the segregation of domains produced a mixture of domains of different sizes. The dynamic equilibrium of the breakup and coalescence finally led to a relatively steady-state domain size and distribution. In comparison with the situation in the initial stage, the domain size was relatively uniform as the mixing proceeded. In Figure 6, a bar diagram of the size distribution is shown. It is obvious that the distribution width decreased rapidly initially and then leveled off. This variation was similar to that of size, and this means that the breakup of the dispersed domains led to not only a small domain size but also a more uniform distribution of sizes. On the whole, this result is similar to the results of our previous study;[23] therefore, Mie scattering is completely valid for describing the morphology development of polymer blends, and further investigations regarding the compatibilization of polymer blends will be discussed with Mie scattering in another article of this series later.

CONCLUSIONS

In this study, the relationship between the phase structure and the blend composition and mixing time was studied by means of SEM and Mie scattering. The results showed that the domain size increased with the concentration of the dispersed phase, and a cocontinuous structure was formed when the PP concentration was between 30 and 50%; this indicated that, in comparison with PS, it was easy to make PP the continuous phase. The results also showed that the initial stage was the main stage of the evolution. In this stage, larger domains of the dispersed phase rapidly broke into smaller ones; accordingly, the size of the domains decreased. The distribution of sizes was also examined; the results showed that the distribution width of sizes decreased initially and leveled off in the late stage of the mixing. Furthermore, results by Mie scattering were similar to those by SEM, confirming the validity of Mie scattering in studies of polymer structure; for this reason, the compatibilization of polymer blends will be discussed with Mie scattering in another article. The main purpose of this article is simply to report this new method.

References

1. Eveaert, V.; Aerts, L.; Groenincks, G. Polymer 1999, 40, 6627.
2. Willemse, R. C.; Ramaker, E. J. J.; van Dam, J.; Posthuma de Boer, A. Polymer 1999, 40, 6651.
3. Fang, Z. P.; Ma, G. W.; Liu, C.; Xu, C. W. J Appl Polym Sci 2004, 91, 763.
4. Hong, J. S.; Kim, J. L.; Ahn, K. H.; Lee, S. J. J Appl Polym Sci 2005, 97, 1702.
5. Halimatudahliana, I. H.; Nasir, M. Polym Test 2002, 21, 263.
6. Joseph, S.; Thomas, S. Eur Polym J 2003, 39, 115.
7. Huneault, M. A.; Champagne, M. F.; Luciani, A. Polym Eng Sci 1996, 36, 1694.
8. Lepers, J.-C.; Favis, B. D.; Tabar, R. J. J Polym Sci Polym Phys 1997, 35, 2271.
9. Scott, C. E.; Macosko, C. W. Polymer 1995, 36, 461.
10. McNally, T.; McShane, P.; Nally, G. M.; Murphy, W. R.; Cook, M.; Miller, A. Polymer 2002, 43, 3785.
11. Favis, B. D. Polymer 1994, 35, 1552.
12. Hamley, I. W.; Stanford, J. L.; Wilkinson, A. N.; Elwell, M. J.; Ryan, A. J. Polymer 2000, 41, 2569.
13. Tol, R. T.; Groenincks, G.; Vinckier, I.; Moldenaers, P.; Mewis, J. Polymer 2004, 45, 2587.
14. Huitric, J.; Mederic, P.; Moan, M.; Jarrin, J. Polymer 2003, 39, 4849.
15. Alcoutlabi, M.; Martinez-Vega, J. J. Polymer 2003, 44, 7199.
16. Kim, J.; Gray, M. K.; Zhou, H. Y.; Nguyen, S. T.; Torkelson, J. M. Macromolecules 2005, 38, 1037.
17. Thomas, S.; Groeninckx, G. J Appl Polym Sci 1999, 71, 1405.
18. Sheng, J.; Qi, L.-Y.; Yuan, X.-B.; Shen, N.-X.; Bian, D.-C. J Appl Polym Sci 1997, 64, 2265.
19. Shih, C. K. Polym Eng Sci 1995, 35, 1688.
20. Zou, J.-L.; Shen, N.-X.; Sheng, J. Acta Polym Sinica 2002, 5, 53.
21. van de Hulst, H. C. Light Scattering by Small Domains; Wiley: New York, 1957; p 119.
22. Beyer, W. H. In Standard Mathematical Tables (in Chinese); Rong, X.-Z., Ed.; Chemical Industry: Beijing, 1988.
23. Li, Y.-Y.; Han, Y.-P.; Zhao, Y.-H.; Sheng, J. J Macromol Sci Phys 2005, 44, 651.